ARTICLES

Electrokinetic displacement of air bubbles in microchannels

Pavlo Takhistov, Alexandra Indeikina, and Hsueh-Chia Chang
University of Notre Dame, Notre Dame, Indiana 46556

(Received 4 October 2000; accepted 10 September 2001)

Displacement of air bubbles in a circular capillary by electrokinetic flow is shown to be possible when the film flow around the bubble is less than the bulk flow behind it. In our experiments, film flow reduction is achieved by a surfactant-endowed interfacial double layer with an opposite charge from the wall double layer. Increase in the film conductivity relative to the bulk due to expansion of the double layers at low electrolyte concentrations decreases the field strength in the film and further reduces film flow. Within a large window in the total ionic concentration C_t, these mechanisms conspire to induce fast bubble motion. The speed of short bubbles (about the same length as the capillary diameter) can exceed the electro-osmotic velocity of liquid without bubble and can be achieved with a low voltage drop. Both mechanisms disappear at high C_t with thin double layers and very low values of zeta potentials. Since the capillary and interfacial zeta potentials at low concentrations scale as $\log C_t^{-1}$ and $\log C_t^{-1/3}$, respectively, film flow resumes and bubble velocity vanishes in that limit despite a higher relative film conductivity. The bubble velocity within the above concentration window is captured with a matched asymptotic Bretherton analysis which yields the proper scaling with respect to a large number of experimental parameters. © *2002 American Institute of Physics.* [DOI: 10.1063/1.1421103]

I. INTRODUCTION

There is considerable interest in using electrokinetic flow for drug delivery through tissues and driving liquids through micron-level channels in microlaboratories and microreactors. Electrokinetic flow occurs when the dielectric channel wall induces a charge separation near its surface such that the counterion concentration decreases away from the wall while the coion concentration increases.[1] Both approach the same value far into the electroneutral bulk electrolyte and there is hence a net charge ρ near the wall. This net charge is confined to a thin double layer of thickness λ, the Debye length specified by a balance between diffusion and potential gradient, and also introduces a normal potential variation within the layer that can be obtained by a simple integration of the Poisson equation. The potential difference across the double layer ζ (zeta potential) is a function of the wall material and the total ionic concentration C_t. In the presence of a tangential external electric field E, this charge separation near the wall introduces a net tangential body force, which is proportional to $E\rho$.

Since the charge ρ is proportional to $d^2\phi/dn^2$ from the Poisson equation and since the tangential force $E\rho$ is balanced by the viscous dissipation $\mu(\partial^2 u/\partial n^2)$, where $\partial/\partial n$ is the normal derivative, the tangential velocity u within the double layer scales as $E\phi$. As a result, the velocity rapidly approaches a constant electrokinetic velocity beyond the thin double layer. Also, since u scales linearly with respect to ϕ and assuming zero slip at the reference point for the zeta potential, one obtains the classical flat electrokinetic velocity profile

$$u_c = -\frac{\varepsilon_0 \epsilon \zeta_c E}{\mu}, \tag{1}$$

where the proportionality constant ϵ is the dielectric permittivity of the medium and the subscript c refers to a cylindrical capillary (our channels of choice) with a diameter d. Hence, as long as the channel size d is much larger than the double layer thickness, this electrokinetic phenomenon acts as a surface force to the bulk fluid that imposes the surface slip velocity (1) at the wall. As a result, the liquid flow rate $u_c A$ is proportional to the channel cross-sectional area $A \sim d^2$, contrary to $\sim d^4$ scaling of the pressure-driven flow, and this is a great advantage for small channels.

In the above-cited applications of electrokinetic flow, parallel transport of long bubbles and organic liquid drops with the electrokinetically driven electrolyte is often desired. The drops can be drugs or blood capsules and the air bubbles can be used to separate samples along channels of microlaboratories. There will be a thin wetting film around these drops/bubbles. Provided such films are much thicker than the capillary double layer, a tangential electric field that drives ions in the double layer will again induce an electrokinetic liquid flow in the film. Unfortunately, the flat electrokinetic velocity profile, which allows effective fluid pumping through small channels, now can become an obstacle. The requirement that the electric current is constant through the capillary and through the film around the bubble (or drop) results in $\sim 1/A$ intensification of the electric field E in the film, where A is the cross-section area of the liquid film around the bubble or drop. If the bubble (drop) interface is mobile (without viscous traction) or the capillary and interfacial zeta potentials are identical, the flat velocity profile (1)

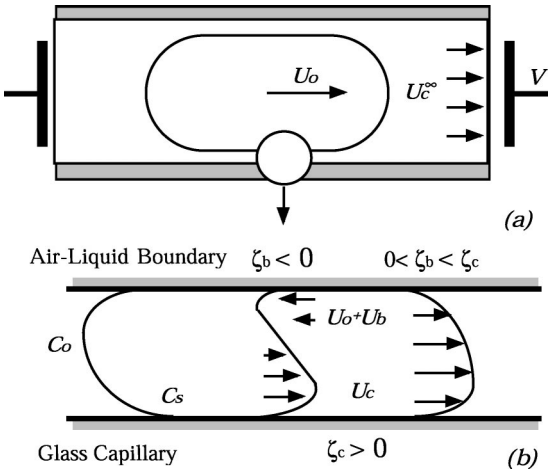

FIG. 1. The structure of double layers and flow inside the film surrounding the air bubble.

of the electro-osmotic flow extends from the capillary double layer across the entire film, as in the capillary behind the bubble. The respective total flow rates, the product of velocity and liquid area, are then identical within the capillary and around the bubble. As a result, the bubble remains stationary while the electrokinetically driven liquid flows around it. Hence, one should somehow reduce the film flow in order to accumulate liquid behind the bubble to build up a pressure gradient, which then displaces the bubble to accommodate the accumulated liquid; and/or introduce interfacial traction such that the electrokinetically driven liquid will drag the bubble along.

The addition of surfactants endows traction on the interface.[2] Ionic surfactants will, however, also introduce a double layer to the interface[3] with a bubble zeta potential ζ_b of the interface different from the capillary zeta potential ζ_c, in general. It is this bubble zeta potential that allows bubble electrophoresis in a bulk liquid. In the thin film, this electrokinetic force drives liquid film flow, as the capillary double layer, but not necessarily in the same direction. Also, if the surfactant concentration is significantly lower than the electrolyte concentration, the capillary zeta potential should not be altered appreciably by the surfactant. Depending on the relative values and signs of the two zeta potentials, these two asymmetric double layers across the film will produce a normal electrokinetic velocity gradient across the film and, hence, can reduce the flow rate below that of a flat velocity profile if the corresponding bubble surface slip electrokinetic velocity u_b is lower than its counterpart u_c on the capillary [see Fig. 1(b)]. This implies that the liquid flow behind the bubble exceeds that around the bubble. As a result, a backpressure builds up behind the bubble to push it forward. In the frame of reference moving with the bubble, the flow rates again balance. The fluid velocity near the bubble interface, u_0+u_b, should never be negative and larger than u_c in magnitude, as this would induce a net negative film flow in the laboratory frame, opposite from the flow upstream of the bubble. By such reasoning, the largest bubble speed would occur when ζ_b and ζ_c are large but of different signs—the capillary and bubble double layers are oppositely charged.

In the present work, we study experimentally and theoretically, following the classical Bretherton problem of pressure-driven bubble transport,[4] the possibility of displacing air bubbles by an electrokinetically driven electrolyte solution in a cylindrical capillary [see Fig. 1(a)]. We have carried out experiments with air bubbles in KCl/H_2SO_4 solutions in a capillary (3 cm length, radius $R=0.25$ mm, the measured ζ_c is positive, indicating a negatively charged double layer) over ranges of KCl concentrations C_0 (10^{-6}–10^{-2} mol/l), air bubble lengths l_b (1.6–20 R) and applied voltages (10–120 V). At such electrolyte concentrations, complete dissociation is expected. We observe bubble motion only after 2×10^{-5} mol/l of SDS (anionic surfactant which induces a positively charged interfacial double layer with $\zeta_b<0$) is added to the solution and only within specific windows of applied voltage (20–80 V) and KCl concentration (10^{-5}–10^{-3} mol/l), with an optimal concentration of 10^{-4} mol/l where the bubble velocity is at its maximum. Bubbles can move with wide-ranging speeds over four orders of magnitude, including an astonishing maximum of 3 mm/s for the shortest bubbles with length $l_b \lesssim 2R$. This high end is comparable to the electroosmotic velocity of KCl solution without the air bubble. In contrast, the introduction of a single bubble increases the required pumping pressure by orders of magnitude in pressure–driven flow.[5] This suggests bubble transport in microchannels is only feasible with properly designed electrokinetic flow.

Using a modified version of Bretherton analysis which includes transport within the double layers, we obtain satisfactory prediction of the bubble speed as a function of l_b, zeta potentials, voltage applied, and the total ionic concentration C_t, which is the sum of the surfactant and electrolyte concentrations. We show that, while the presence of interfacial traction is necessary for bubble transport, the window in electrolyte concentration where bubble motion is possible and the bubble speed are mostly determined by the effective drag from asymmetric double layers. The increase in the film conductivity relative to the bulk caused by double layers expansion at low electrolyte concentrations ($C_0<10^{-3}$ mol/l) and the resulting decrease in film electric field are shown to be responsible for the observed fast bubble motion. Correspondingly, the vanishing double layer thickness and the decrease in the absolute values of the zeta potentials with increasing concentration define the upper concentration bound for bubble motion. At very low concentrations, the positive electrokinetic flow at the capillary exceeds the negative flow at the interface, again permitting positive film flow and slow bubble speed. At these low concentrations, however, the film around the bubble cannot be sustained because of unscreened electrostatic attraction between oppositely charged bubble interface and capillary wall. This results in breaking the electric current through the film and produces the lower concentration bound for bubble motion.

II. EXPERIMENTS

Two open acrylic electrode chambers are connected to both ends of a horizontal glass capillary tube with diameter $d=0.5$ mm and length $L=3$ cm. The chambers house two

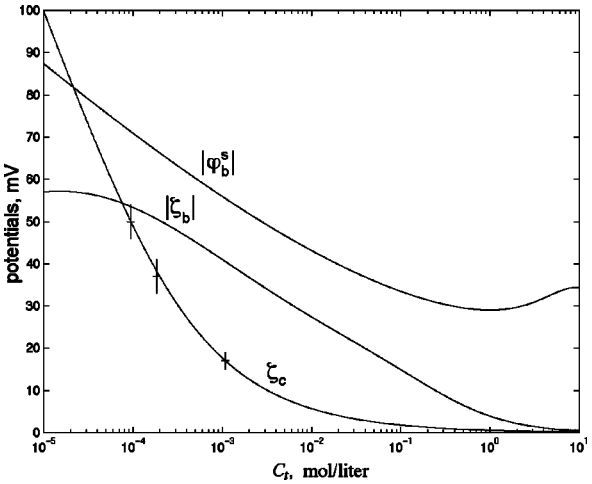

FIG. 2. The dependence of zeta potentials ζ_c and ζ_b and bubble interfacial potential φ_b^s on total electrolyte concentration from our measurements and model. Both bubble zeta potential ζ_b and interfacial potential φ_b^s are negative for our anionic SDS surfactant.

platinum foil electrodes. The chambers and connecting capillary are filled with a working electrolyte solution, KCl/SDS with a small addition of sulfuric acid. The H_2SO_4 concentration C_a remains constant for all experiments at $C_a = 3.62 \times 10^{-5}$ mol/l. The KCl concentration C_0, however, ranges from 10^{-6} to 10^{-2} mol/l. For all experiments with SDS, the surfactant concentration is $C_s = 2 \times 10^{-5}$ mol/l. We do not measure the surface tension for our working solution and use an estimated value of $\sigma = 60$ dyn/cm in our subsequent analysis.

Before each new series of experiments, the capillary is carefully cleaned with distilled water and ethyl alcohol and then thoroughly rinsed first with distilled water and finally with the electrolyte solution. When the electrolyte concentration is changed, the capillary is filled for 24–48 h to achieve equilibrium at the surfaces. We found such careful preparation necessary for reproducible data, presumably because of extraneous surface ionic charges that may distort the double layers.

We have also measured the capillary zeta potential in our working KCl/H_2SO_4/SDS solutions. The working capillary is connected in series with two open-end capillaries of the same diameter by two electrode chambers. All sections are carefully aligned on the same horizontal level. When a potential difference is applied to the electrodes, electro-osmotic flow develops in the test section and results in meniscus motion in the outer open-end capillaries, which is captured with a video camera. The measured meniscus speed then provides the electro-osmotic velocity u_c. The known voltage drop across the test section allows us to invoke Eq. (1) and find the capillary zeta potential.

As seen in Fig. 2, the zeta potential for our capillary is positive and its dependence on the total ionic concentration of the solution is well represented by the model of constant surface charge to be presented in a subsequent section. (By the usual convention, zeta potential has the same sign as the surface charge.[6] The dominant ions in the double layer hence have an opposite charge—anions in our capillary double layer.) Most glasses are negatively charged but exceptions with sodium dopant for electrode casings are known to be positively charged (see Ref. 3, p. 96 and Ref. 7, p. 115). The measurements in Fig. 2 are done in the presence of the anionic surfactant SDS. However, the dilute amount of SDS (2×10^{-5} mol/l) does not seem to alter the positive surface charge in the presence of more concentrated electrolyte buffer. To neutralize or reverse the surface charge, the SDS and/or electrolyte buffer concentration would need to be several orders of magnitude larger. (The explanation of charge reversal mechanism and typical values of required counterions concentrations may be found in Ref. 6, pp. 84–89.)

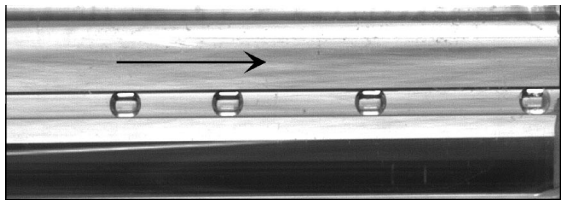

FIG. 3. The position of a single air bubble at different moments of time from overlapping images. The arrow shows the direction of motion.

The air bubble is introduced into the capillary with a microsyringe. After waiting for about 1 h, a voltage is applied to the platinum electrodes in both chambers and the bubble motion is monitored. This waiting period is necessary to equilibrate the annular liquid film around the bubble and/or interfacial double layer to ensure reproducible data on bubble velocity. If the voltage is applied immediately after bubble placement, there is no detectable bubble motion in most cases, but sometimes the bubble starts to move very fast after several minutes. We image the bubble motion with a high-resolution Kodak MegaPlus 1.6 digital camera (see Fig. 3). The location and speed of the transporting bubble are obtained through standard software packages. The measurements are stopped when the bubble reaches the end of the capillary. A new bubble is used after each traverse.

We also measure the overall electric resistance of our experimental cell with and without bubble by a digital multimeter DM-350A. The voltage drop in the electrode chambers is estimated to be negligible, and the resistance occurs mostly across the capillary. With bubble, both the surrounding film and the bubbleless portion of the capillary contribute to the total resistance. Measurement of the electrical resistance is carried out about 5 min after bubble placement, when the bubble is motionless. The overall resistance is independent of the bubble location. It is, however, sensitive to the bubble length l_b due to high film resistance. The measured total resistance R_b, normalized with respect to the bubbleless capillary resistance R_0, is shown in Fig. 4 as a function of the length of the motionless bubble. While the overall resistance increases up to the 50 times for the longest bubble, a measurable current still passes through the system, indicating the thickness h of the film surrounding the bubble does not approach zero in the limit of stationary bubbles when the bubble velocity u_0 vanishes. This is in contradiction to the Bretherton theory[4] that predicts h to scale as $u_0^{2/3}$. However, Chen[8] has shown experimentally that grooves

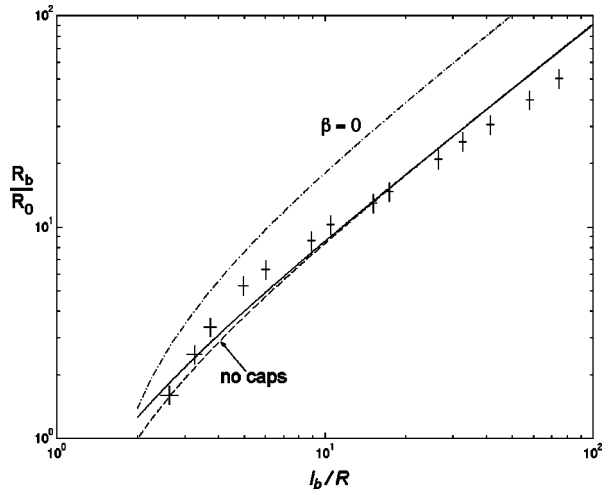

FIG. 4. Relative resistance of capillary tube filled by electrolyte with an air bubble as a function of bubble length ($C_0=10^{-4}$ mol/l). The theoretical curves correspond to our full model and its two limits—without double layer conductivity ($\beta=0$) and without cap resistance.

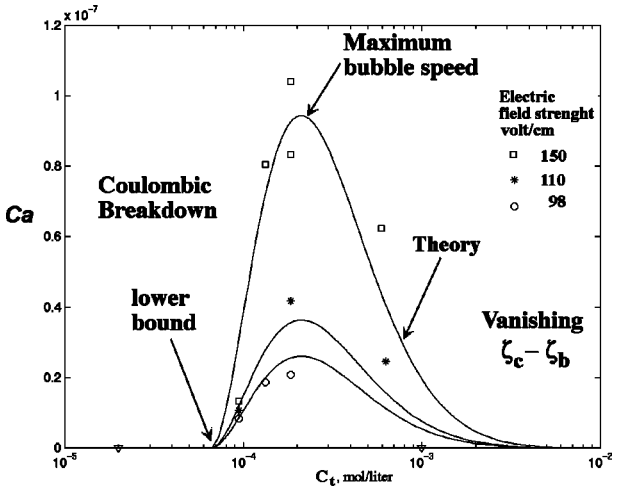

FIG. 6. The dependence of Ca on the total ion concentration.

along the capillary and intermolecular forces can still sustain a very thin film with a limiting thickness h_0 of about 0.7 μm. We shall use our resistance data for motionless bubbles to confirm our theory for electric fields around and away from a moving bubble.

Without adding surfactants to the electrolyte solutions, there is no detectable motion for any bubble. The presence of a cationic surfactant (CTAB), which produces negatively charged interfacial double layer like the capillary double layer, also does not induce bubble transport. Bubble motion is detected after $C_s=2\times10^{-5}$ mol/l of anionic surfactant (SDS) is added and only within the windows of KCl concentrations (10^{-5}–10^{-3} mol/l) and applied voltages (20–80 V). This anionic surfactant should produce a positively charged interfacial double layer and a negative zeta potential opposite from our measured capillary zeta potential. The measured bubble velocity u_0 as a function of voltage V and KCl concentration C_0 are shown in Figs. 5 and 6 for several bubble lengths l_b. Strong dependence on C_0, V, and l_b is evident. Especially dramatic is the rapid increase in u_0 with decreasing C_0, followed by an abrupt cessation of bubble motion below $C_0^c=10^{-5}$ mol/l (or $C_t^c=0.948\times10^{-4}$ mol/l) and a similar increase with respect to V followed also by a cessation beyond $V_c=80$ V. Both conditions, below C_0^c and beyond V_c, are accompanied by a complete current stop. In fact, film boiling is observed beyond V_c, and the appearance of dry spots suppresses the electric current and hence the bubble motion. In contrast, at high electrolyte concentrations, beyond $C_0=10^{-3}$ mol/l, electric current remains measurable, even though the bubble is motionless. There are hence different mechanisms that define the two bounds of operating conditions when bubble motion can be electrokinetically driven. As evident from Figs. 5 and 6, these windows in C_0 and the applied voltage seem to be independent of bubble length. The potential where the bubble speed saturates decreases with bubble length, in contrast to the length-independent location of the optimal concentration for maximum speed.

The bubble velocity u_0 is, however, a strong function of l_b and this dependence is further explored in the data pre-

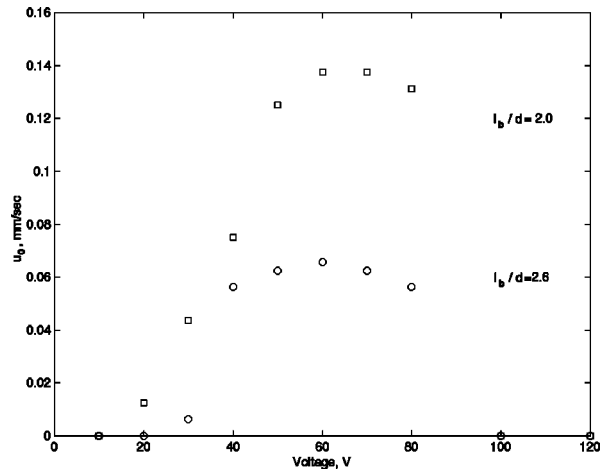

FIG. 5. Dependence of bubble velocity on the applied voltage ($C_0=10^{-4}$ mol/l). (□) $l_b/R=4$ and (○) $l_b/R=5.2$.

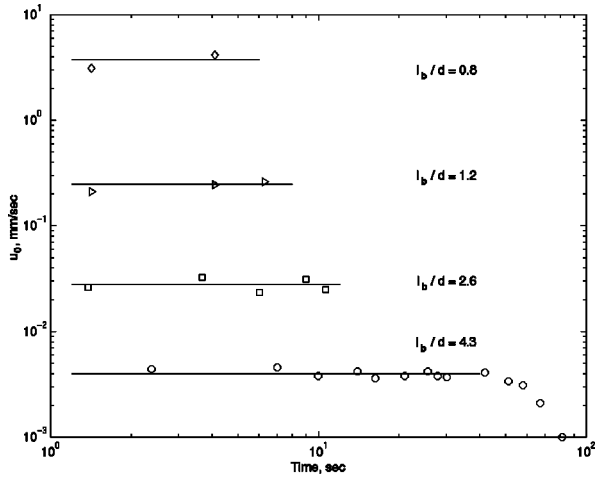

FIG. 7. Time history of the bubble velocity as a function of bubble length. $C_0=10^{-4}$ mol/l, $V=42$ V.

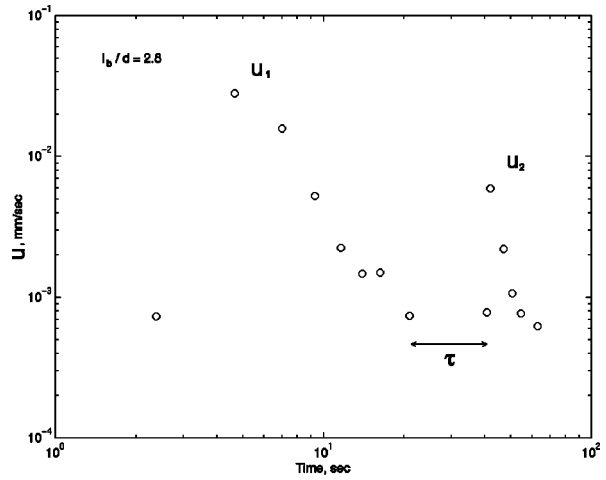

FIG. 8. The influence of voltage stoppage on the velocity of decelerating bubbles. $C_0 = 10^{-4}$ mol/l, $V = 42$ V.

sented in Fig. 7. For short bubbles ($l_b/R \lesssim 4$), the motion reaches a steady speed after a very short transient and maintains that value throughout the length of the capillary. For $l_b/R \sim 1.6$ this steady speed could reach exceedingly high values of $u_0 = 3$ mm/s. This steady speed drops precipitously with bubble length such that for $l_b/R = 8.6$, u_0 is as low as 4×10^{-3} mm/s. Moreover, long bubbles with $l_b/R > 5$, can decelerate after some period of steady motion. The duration with constant speed and the rate of decrease in velocity depend on the bubble length, applied voltage and electrolyte concentration.

If the applied voltage is removed temporarily, the velocity u_2 after the voltage is reapplied is higher than the bubble speed when it is removed but lower than the original value u_1 before deceleration. This is evident in the run shown in Fig. 8 where a 20 s stoppage is introduced at $t = 20$ s into the experiment. The scaling law shown in Fig. 9 suggests that ion diffusion is responsible for this phenomenon, as will be discussed subsequently.

The results for decelerating bubbles are, however, hardly reproducible and, at the present time, we have no reliable

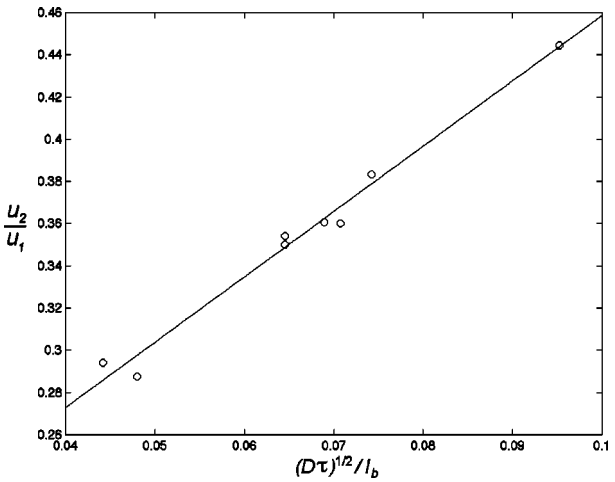

FIG. 9. Velocity jumps after reapplying voltage. $C_0 = 10^{-4}$ mol/l, $V = 42$ V, delay time τ is in the range of 10–25 s, $l/R = 6-16$.

data to quantify the time evolution of bubble speed. Also, the length of our capillary is too small to draw a definite conclusion about the temporally varying velocity of shortest bubbles, with $l_b/R \approx 2$, i.e., does the acceleration detected in some experiments really exist? Nevertheless, it is established that the average bubble speed decreases rapidly with increasing bubble length.

III. PHYSICAL MECHANISM OF BUBBLE TRANSPORT

Our explanation of how the bubble speed depends on V, C_0, and l_b will be based mostly on the asymmetric double layers and their effect on film conductivity, sketched in Fig. 1(b). The necessity of interfacial traction for bubble transport has already been outlined in Sec. I, and our experiments confirm the proposed scenario—without surfactant, no bubble motion is detected.

Since the addition of the anionic surfactant (SDS) introduces negative charges on the liquid–air interface ($\zeta_b < 0$), and our measurement of electro-osmotic velocity in the bubbles capillary indicates a positively charged capillary wall ($\zeta_c > 0$), double layers on the air–liquid interface and the capillary pull the film in opposite directions and the film velocity profile resembles that shown on the left-hand side of Fig. 1(b). If interfacial mobility and the values of zeta potential allow complete cancellation of film flow, the bubble will move as in the pressure-driven case, with speed specified by the liquid velocity in the capillary away from the bubble. This motion for long bubbles ($l_b/R \gtrsim 4$), however, would be very slow and probably undetectable in our experiments. As stipulated by the resistance measurements in Fig. 4, most of the applied voltage is required to provide the current through the film, and almost nothing would be left to drive the fluid in the capillary for pressure-driven bubble motion. If $|\zeta_b| > \zeta_c$ (which is indeed true for the observed bubble motion window) and the increase in total resistance is not very significant because of the small bubble length and/or the high film conductivity, the additional driving force on the bubble due to the interfacial double layer can dominate. This negative electrokinetic flow on the interface can actually produce a net ejection of liquid behind the bubble. This liquid and the forward moving bulk from behind can build up a back pressure much larger than that of the Bretherton bubble with no flow through the film. As a result, short bubbles will move faster than electrolyte in a bubbleless capillary under the same experimental conditions (V and C_0). In contrast, the addition of cationic surfactant (CTAB) produces the same interfacial charge as that of capillary wall, and the resulting reduction of the film flow [sketched on the right-hand side of Fig. 1(b)] may be insufficient to induce detectable bubble motion.

Consider now the dependence of bubble speed on concentration. At low electrolyte concentrations (below 10^{-3} mol/l), the average ion concentration in the film becomes different from that away from the bubble. In the middle of the film, away from both double layers, the ion concentration is equal to the bulk concentration C_t behind and ahead of bubble. However, concentrations within the double layers are much higher due to stoichiometrically disproportional excess

of counterions. The Boltzmann relation between surface and bulk concentrations, which follows from a thermodynamic equilibrium across the double layer, suggests that the ionic concentration near the interface can be 10–100 times C_t, depending on values of the zeta potential and valency of the counterion. Since the double layer thickness $\lambda \sim C_t^{-1/2}$, the ratio between the average concentration across the film and C_0 increases significantly as the bulk region of the film becomes comparable in thickness to the double layers. This large ionic concentration in the film increases the conductivity, decreases the voltage drop across the bubble and hence further decreases the film flow relative to the capillary. Moreover, as we shall demonstrate in Sec. IV, both interfacial and capillary zeta potentials increase in absolute value with decreasing C_t (see Fig. 2) which, if they are of different signs, also enhances the flow imbalance and hence increases the bubble speed. We will also show that enhancement of film conductivity has a dramatic effect on bubble speed. Neglecting this effect results in speeds about two orders of magnitude lower than the measured values—it is hence the dominant mechanism for high-speed bubble transport at low C_t.

At high ionic concentrations, the vanishing thickness of the double layers (compared, for example, with approximately 0.7 μm film thickness under the motionless bubble[8]) and low values of zeta potential (only 17 mV for our capillary at 10^{-3} mol/l) rule out all these flow-reduction mechanisms. This accounts for the upper bound of the bubble motion window.

Consider now the opposite limit of very low concentrations, when the double layers can overlap within the film. Under these conditions, several effects come into play. First of all, interfacial zeta potential endowed by ionic surfactant and capillary zeta potential have different dependence on the total ionic concentration C_t.[6] In Fig. 2, we show our computed bubble interfacial potential φ_b^s and zeta potential ζ_b as a function of C_t. The theory will be presented in Sec. IV and is based on literature data for SDS absorption on an air/water interface in the presence of added electrolyte. Figure 2 also contains the measured capillary zeta potential and the calculated extrapolation, based on a constant charge model [$z = 4eC_t\lambda \sinh(e\zeta_c/2kT) = \text{const}$] to be presented in Sec. IV. It is evident that both of them increase in absolute value with decreasing C_t, but below $C_t = 7.5\times10^{-5}$, ζ_c becomes larger than $|\zeta_b|$. This reverses the asymmetric double layer effect and the bubble speed decreases.

The condition $\zeta_c = |\zeta_b|$ actually produces the low Bretherton velocity with no film flow. Moreover, while the concentration of the electrolyte decreases, the surfactants still endow the bubble interface with a charge. Hence, it is quite possible that if the film thickness drops below several Debye lengths, the film will simply collapse due to the Coulombic attractive force between differently charged surfaces—the interface and the capillary. There is hence a very specific cutoff at low concentrations for bubble motion.

IV. MODEL

Estimate of the bubble velocity u_0 requires knowledge of the film flow and film velocity profile which, in turn, are specified by the film electric field, ion concentration, and the film thickness h. The film thickness is determined by how capillary pressure and electrokinetic flow drive fluid from the caps into and out of the film. Due to the extra curvature at the front cap, a positive capillary pressure gradient exists there to oppose the electrokinetic flow into the film. This necessitates a Bretherton-type analysis[4] for bubble motion in capillaries. We will mostly focus on the motion of long bubbles, where the flat portion of the film is significantly larger than the caps regions. This separation of length scales allows a simplifying matched asymptotic analysis.

A. Hydrodynamics

Ionic surfactants, in the presence of the imposed external electric field, produce significant Marangoni effects—at least a factor of 3 larger than their nonionic analog.[6] We hence assume that the bubble interface is immobile, such that the liquid velocity at the interface is equal to the bubble velocity u_0, and the interfacial double layer drives liquid relative to the bubble in the same manner as near a solid particle. Ratulowski and Chang[2] have shown that the above immobile limit is reached when there is a very large Marangoni effect. The immobile film of the pressure-driven Bretherton problem sustains no flow but this is not true for electrokinetic flow. The above immobile assumption probably will not work for liquid drops because of the possibility of internal liquid motion, which has been shown to greatly increase the electrokinetic velocity of mercury drops.[9]

With the usual thin film lubrication assumptions,[1] the electrokinetic velocity profile in the film and in the transition region from the film to the caps becomes to leading order:

$$u = \frac{\epsilon\varepsilon_0\Phi_x}{\mu}\left(\zeta_c - \varphi + \frac{y}{h}[\zeta_b - \zeta_c]\right) - \frac{P_x}{2\mu}(yh - y^2) + \frac{u_0 y}{h}, \tag{2}$$

where the boundary conditions, u is zero at $y=0$ and u_0 at $y=h$ and the potential φ is equal to the capillary zeta potential ζ_c and bubble zeta potential ζ_b at $y=0$ and h, have been imposed. In Sec. IV B, we shall distinguish between the interfacial potential φ_b^s and the bubble zeta potential ζ_b, which are evaluated at a distance of several molecular diameters apart across the immobile part of the double layer. This distance is, however, indistinguishable for the hydrodynamic description of film flow and we have applied the no-slip conditions at the capillary wall $y=0$ and at the bubble interface $y=h$. In (2), we decompose the total potential $\phi(x,y)$ into two parts:

$$\phi = \Phi(x, y/h) + \varphi(x, y/\lambda), \tag{3}$$

where Φ represents the potential of electroneutral solution in the bulk of the film, and φ corresponds to the potential induced by charge separation in the double layers. In the film and the transition region $\Phi \approx \Phi(x)$ while $\varphi \approx \varphi(y)$, such that $\varphi(0) = \zeta_c$ and $\varphi(h) = \zeta_b$. Nevertheless, we keep the general dependence in (3), as well as the $-\varphi$ term in (2), anticipating discussion of the short bubble motion and consideration of thin film thickness h comparable to the double layer thickness.

For electrolytes in the presence of an electric field, the

pressure term in (2) should also be modified compared to the usual pressure-driven flows and becomes:[10,7]

$$P = P_{\text{gas}} - \sigma\left[h_{xx} + \frac{1}{R-h}\right] - \frac{\epsilon\varepsilon_0}{2}\Phi_x^2 - \Pi. \tag{4}$$

The second term in (4) corresponds to the usual capillary pressure while the third term is a Maxwell pressure on the boundary between two dielectrics in the presence of the tangential electric field,[10] and hence have the same origin as $\sim \nabla\phi\nabla^2\phi$ term in the Navier–Stokes equation for electrolyte flow in an electric field.[7] The disjoining pressure Π becomes significant for thin films. It contains the usual van der Waals term $\Pi_{\text{vdW}} = -A/6\pi h^3$, where A is the Hamaker constant (A is negative for systems air/wetting fluid/solid, such that $\Pi_{\text{vdW}} > 0$ and the interaction is repulsive) and electrostatic attraction/repulsion between oppositely/similarly charged double layers.[11,3] The gas pressure P_{gas} and the azimuthal curvature $1/(R-h) \approx 1/R$ in (4) do not vary longitudinally in the film and hence do not contribute to the gradient P_x in (2) as a driving force for the flow.

In the capillary away from the bubble, the flat velocity profile is defined by Eq. (1) with the electric field strength $E = -\Phi_x^\infty$ which, as well as the film field strength $-\Phi_x(x)$, needs to be related to the overall voltage drop, bubble length and other experimental parameters. If the bubble is in steady motion, one must satisfy the flow rate balance through the film and capillary in the frame of reference moving with the bubble speed u_0:

$$2\pi R\left\{\int_0^h u(y)dy - u_0 h\right\} = \pi R^2(u_c^\infty - u_0)$$

$$= \pi R^2\left(\frac{\varepsilon_0\epsilon}{\mu}\zeta_c^\infty\Phi_x^\infty - u_0\right), \tag{5}$$

where the superscript ∞ refers to the values at the capillary away from the bubble, R is the capillary radius, and the liquid velocity in the film is given by (2).

The Bretherton problem for a pressure-driven bubble with completely immobilized interface corresponds to $P_x = -\sigma h_{xxx}$ and $u(y)$ from (2) with the first electrokinetic term omitted. With h scaled by the flat-film thickness h_0R and x by $x_0 = h_0R(6\,\text{Ca})^{-1/3}$ (the capillary number $\text{Ca} = \mu u_0/\sigma$ is the dimensionless version of the bubble speed), the flow rate balance (5) gives the bubble velocity

$$u_0 = u_c^\infty/(1-h_0) \approx u_c^\infty \tag{6}$$

and the classical Bretherton equation[4] for the interfacial shape in the transition region

$$h_{xxx} = (h-1)/h^3. \tag{7}$$

Since the bubble interface is no longer mobile, the film flow rate is different from that for stress-free bubble and the scaling for x has a factor of $(6\,\text{Ca})^{-1/3}$ instead of Bretherton's classical $(3\,\text{Ca})^{-1/3}$ (see Ratulowski and Chang[2] for related scaling variations). Integrating (7) forward yields a unique quadratic blow-up behavior

$$h(x\to\infty) = 2.898 + 0.643\,42\frac{x^2}{2}, \tag{8}$$

where the linear term has been suppressed by a proper choice in the origin of x. The asymptotic curvature of this inner solution in dimensional coordinates must match with the $1/R$ curvature of the front cap which also makes quadratic tangent with the capillary. Matching the two yields the immobile bubble version of the classical Bretherton result for the pressure-driven flow,

$$h_0 = 0.643\,42(6\,\text{Ca})^{2/3}. \tag{9}$$

There are, however, limiting conditions when the electrokinetic flow problem reduces to the classical one. If the Maxwell and disjoining pressures in (4) are negligible and if $\zeta_b = -\zeta_c$, it is clear that the electrokinetic term in (2) does not contribute to the flow rate, regardless of the field strength $\Phi_x(x)$. Equations (6) and (9) then provide the relations between the bubble speed u_0, fluid velocity in the capillary u_c^∞, and the film thickness h_0R. We will show that similar simplification also occurs at high ionic concentrations, when the double layer potential φ is negligible and $\Phi_x(x) \sim 1/h(x)$, such that only a constant is added to the flow rate balance (5). In both cases, however, the fluid velocity in the capillary u_c^∞ is not the externally imposed speed of a driving piston, as in typical experiments on the pressure-driven bubble transport. Instead, it is defined by the field strength in the capillary Φ_x^∞ which, in turn, depends not only on the overall potential drop, bubble length, and concentrations but also on the film thickness (9) and these dependences still remain to be determined.

B. Concentrations profiles in the film and zeta potentials

To pursue the electrokinetic flow case, we must resolve the potentials φ and Φ and find the dependence of the zeta potentials on the electrolyte concentration. Because our experimental system contains only strong electrolytes at concentrations below 10^{-3} mol/l, we assume complete dissociation of all ionic species. For simplicity, we will present an analysis only for 1:1 electrolyte. To apply this model to our KCl/H_2SO_4 system, we shall combine them into a model electrolyte with both ions having unit valency. The bulk concentration C_e of this model electrolyte is the sum of the KCl concentration C_0 and $2C_a$, twice the H_2SO_4 concentration.

We expect that the concentrations of K^+, Cl^-, H^+, SO_4^{2-} and the two surfactant ions in the middle of the film to be different from their counterparts in the bulk away from the bubble. This difference is due to adsorption/desorption from the film and double layers. However, it is not feasible to model all these complex transport and kinetic phenomena. (Some models for a single surfactant are available in Ratulowski and Chang.[2]) Instead, we assume that, in the limit of thin double layers relative to the film, the bulk concentrations of each ion within the electroneutral part of the film are equal to their counterpart in the capillary away from the bubble.

There are hence two bulk concentrations—the model electrolyte concentration $C_e = C_0 + 2C_a$ and the surfactant concentration C_s. The total bulk ion concentration $C_t = C_e + C_s$. We invoke a Boltzmann equilibrium approximation for all ions within the film, which gives

$$C^{\pm}_{e,s,t} = C_{e,s,t} \exp\left(\mp \frac{e\varphi(y)}{kT} \right). \tag{10}$$

In our case of oppositely charged interfaces the local potential $\varphi(y)$ always changes sign within the film unless the ionic concentration becomes unrealistically low that one double layer completely suppresses another. Consequently, the bulk values C_e, C_s, and C_t at the middle of the film are the proper reference concentrations for (10).

The Poisson equation for the nondimensional local potential $\varphi' = e\varphi/kT$ is then

$$\varphi_{yy} = \frac{1}{\lambda^2} \sinh\ \varphi, \tag{11}$$

where the prime is omitted and $\lambda = (\epsilon\varepsilon_0 kT/2C_t e^2)^{1/2}$ is the Debye length. Its boundary conditions on the capillary wall and bubble interface are

$$\frac{z_c}{e} = -2C_t\lambda^2\varphi_y(y=0), \quad \frac{z_b}{e} = 2C_t\lambda^2\varphi_y(y=h), \tag{12}$$

where $z_{c,b}$ are the corresponding interfacial charge densities (for our system $z_c > 0$ and $z_b < 0$). Solution of (11) then specifies the potential and concentration distributions within the film. Equation (11) can be easily integrated once to give

$$\varphi_y^2 = \frac{4}{\lambda^2} \sinh^2\ \varphi/2 + A, \tag{13}$$

where the integration constant A for our case of oppositely charged interfaces corresponds to the squared field strength, φ_y^2, within the film at the position where φ vanishes.

Equations (13) and (12) allow closed-form analytical solution only for noninteracting double layers, i.e., when one of the boundary conditions (12) is replaced by the trivial one at infinity. This noninteracting double layer limit gives $A = 0$. This approximation is definitely valid for the bubbleless capillary (because $\lambda \ll R$, see Probstein,[1] for example) such that one obtains a relation between the interfacial charge density z_c and interfacial potential φ_c^s and an expression for the potential distribution within wall double layer:[1,11,12]

$$\frac{z_c}{e} = 4C_t\lambda\ \sinh\frac{\varphi_c^s}{2}, \quad \tanh\frac{\varphi_c}{4} = \tanh\frac{\varphi_c^s}{4}\exp\left(-\frac{y}{\lambda}\right). \tag{14}$$

The electrokinetic potential ζ_c corresponds to the value of φ_c at a distance of about 3–4 molecular diameters from the wall. Numerous experimental data[3,12] suggest that, for most glasses, ζ_c and φ_c^s are almost indistinguishable for our working range of electrolyte concentrations. The wall charge density z_c is determined only by the material properties and is hence a constant independent of the electrolyte and/or the presence of external electric field. Hence, we use (14) with $\varphi_c^s = \zeta_c$ to fit out data on capillary zeta potential. As seen in Fig. 2, the agreement is excellent, even for low KCl concentration, where the error introduced by the model 1:1 electrolyte is expected to be the most significant. Surprisingly, exact solutions for the KCl/H_2SO_4 system, both with complete ($H_2SO_4 \rightarrow 2H^+ + SO_4^{2-}$) and partial ($H_2SO_4 \rightarrow H^+ + HSO_4^-$) dissociation, give worse results.

The charge density on the air/liquid interface, however, is specified by the interfacial surfactant concentration $\Gamma = -z_b/e$ and hence by the adsorption/desorption from the film. At equilibrium, Γ for anionic surfactant is determined by[6]

$$\Gamma = k_n \exp\{\varphi_b^s + a_n\sqrt{\Gamma}\} C_s(1 - \Gamma/\Gamma_\infty), \tag{15}$$

where $\Gamma_\infty \approx 3\times10^{14}$ cm^{-2} is the number of water sites per unit area of the interface, and the constants k_n and a_n depend on adsorption energy per CH_2 group, length of the hydrocarbon chain, and other factors. (For SDS at air/water interface at room temperature, $k_n \approx 4.85\times10^{18}$ cm^{-2} l/mol and $a_n \approx 3.5\times10^{-7}$cm.) On the other hand, Γ and φ_b^s for the single air/liquid interface are related through (14) with an appropriate change of notation,

$$\Gamma = -4C_t\lambda\ \sinh\frac{\varphi_b^s}{2}, \quad \tanh\frac{\varphi_b}{4} = \tanh\frac{\varphi_b^s}{4}\exp\left(-\frac{h-y}{\lambda}\right). \tag{16}$$

Hence, the interfacial potential depends both on C_t and C_s, and that parametric dependence can be deduced from Eqs. (15) and (16). In the limit of low Γ and large $|\varphi_b^s|$ ($\Gamma \ll \Gamma_\infty$, $a_n\Gamma \ll 1$, and $-\sinh\varphi_b^s/2 \approx 0.5\exp|\varphi_b^s/2|$, which corresponds to the dimensional $|\varphi_b^s|$ in excess of 100 mV), it reduces to

$$\Gamma \approx k_\Gamma (C_s C_t)^{1/3}, \quad |\varphi_b^s| \approx \log\frac{k_n}{k_\Gamma} + \frac{2}{3}\log\ C_s - \frac{1}{3}\log\ C_t, \tag{17}$$

where $k_\Gamma = (2k_n\epsilon\varepsilon_0 kT/e^2)^{1/3} \approx 1.87\times10^{15}\text{cm}^{-2}(\text{l/mol})^{2/3}$. It is shown[6] that this limiting equation is a good description for SDS adsorption from water or from water/NaCL solutions for moderate surfactant concentrations (10^{-4}–10^{-3} mol/l).

Contrary to the glass surface, electrokinetic potential ζ_b at air/liquid interface differs significantly from interfacial potential φ_b^s even at low electrolyte and surfactant concentrations,[3] probably due to the large size of the surfactant molecules (about 2.5 nm) and the dynamic nature of the adsorption/desorption equilibrium at the interface. Moreover, the degree of interfacial dissociation and hence k_n depend on the underlying electrolyte, especially on the pH. As a result, typical measured values for $|\zeta_b|$ are about 30%–50% lower than $|\varphi_b^s|$ calculated using Eqs. (15) and (16).

Unfortunately, we did not find experimental data on both ζ_b and φ_b^s for our experimental system. Hence, to model the dependence of bubble zeta potential on concentrations of the ionic species for our system, we use the adsorption equilibrium of positive ions on the available surfactant sites to estimate the interfacial concentration Γ^+ of positive ions, which is also related with the potential φ_b^{st} at the Stern plane,

$$\Gamma^+ = [k_e(C_0 + C_s) + k_a 2C_a]\exp\{-\varphi_b^{st}\}\frac{\Gamma - \Gamma^+}{\Gamma_\infty},$$
$$\Gamma - \Gamma^+ = -4C_t\lambda\ \sinh\frac{\varphi_b^{st}}{2}. \tag{18}$$

The electrokinetic potential ζ_b should then be evaluated at a distance d_{eff} from it. By assuming the dependence of d_{eff} on the molecular size and concentrations as

$$d_{\text{eff}}=\frac{m_1 m_2 d_{se}\lambda}{m_1 d_{se}+m_2\lambda}, \quad d_{se}=d_e+(d_s-d_e)\frac{C_s}{C_t}, \tag{19}$$

one obtains from (15), (16), and (18) the implicit dependence of φ_b^{st} on C_t and C_s, and also the dependence of zeta potential ζ_b,

$$\tanh\frac{\zeta_b}{4}=\tanh\frac{\varphi_b^{\text{st}}}{4}\exp\left(-\frac{d_{\text{eff}}}{\lambda}\right). \tag{20}$$

In (19), $d_e=0.66$ nm and $d_s=2.5$ nm are the typical effective ionic diameter and the length of the hydrocarbon tail for SDS, respectively.[11] The values of constants k_e and k_a in (18) and m_1 and m_2 in (19) are determined by fitting available experimental data[3,6] on ζ_b at different C_s, C_0, and pH of the solution. The results for our experimental system are shown in the Fig. 2 ($k_e=3.6\times10^{14}$ cm^{-2} l/mol, $k_a=6\times10^{16}$ cm^{-2} l/mol, $m_1=3.5$, $m_2=0.5$), where we show the dependence of $|\varphi_b^s|$ and $|\zeta_b|$ on the total electrolyte concentration C_t. (The surfactant and acid concentrations C_s and C_a are fixed in our experiments.)

C. Flow rate balance

Within the working range of concentrations both $|\zeta_b|$ and ζ_c for isolated interfaces do not exceed 60 mV (2.4 in kT/e units). We can hence invoke the approximation of weakly interacting double layers[11] to determine the integral of double layer potential across the film, which is needed to complete the flow rate balance (5). Under the assumption of $|\tanh\varphi/4|\ll1$, the potential profile within the film is then given by the superposition of the solutions of (14) and (16) from isolated interfaces,

$$\gamma\left(\frac{y}{\lambda}\right)=\tanh\frac{\varphi}{4}=\left[\tanh\frac{\zeta_c}{4}\sinh\left(\frac{h-y}{\lambda}\right)+\tanh\frac{\zeta_b}{4}\sinh\left(\frac{y}{\lambda}\right)\right]\Big/\sinh\left(\frac{h}{\lambda}\right), \tag{21}$$

where a new function $\gamma=\tanh(\varphi/4)$ is introduced to simplify the derivation and electrokinetic zeta potentials are chosen as reference values instead of φ^s, such that the boundary conditions $\varphi(0,h)=\zeta_{c,b}$ are applied at the shear planes, similar to Eq. (2). This approximation, however, cannot be extended up to the bubble interface because of the large value of $|\varphi_b^s|$ at low C_t. Noting that the derivative of γ can be written as

$$\gamma_y=-\frac{1}{\lambda}(\gamma^2(y)+A)^{1/2},$$
$$A=\left[\gamma_c^2+\gamma_b^2-2\gamma_c\gamma_b\cosh\left(\frac{h}{\lambda}\right)\right]\Big/\sinh^2\left(\frac{h}{\lambda}\right) \tag{22}$$

(A is positive because $\gamma_b<0$ and $\gamma_c>0$), one can invoke $|\gamma|\ll1$ assumption and approximate the integral of the local potential across the film by

$$\int_0^h\varphi(y)dy=\int_{\gamma_c}^{-|\gamma_b|}\frac{\varphi(\gamma)}{\gamma_y}d\gamma=-4\lambda\int_{\gamma_c}^{|\gamma_b|}\frac{\tanh^{-1}(\gamma)}{(\gamma^2(y)+A)^{1/2}}d\gamma\approx\lambda(|\zeta_b|-\zeta_c)\left[\tanh\left(\frac{h}{2\lambda}\right)+O\left(\gamma^2\exp\left(-\frac{h}{\lambda}\right)\right)\right]. \tag{23}$$

It should be noted that ζ_c and ζ_b in the thin film are, in general, different from those for isolated surfaces, shown in Fig. 2. They depend on h/λ and should be related with interfacial potentials [e.g., $\zeta_c=\varphi_c^s$ and some analog of (19) for bubble] and hence with surface charge densities through the boundary conditions (12) on the interfaces. The surfactant adsorption/desorption on the interface [even at equilibrium, see (15)] make such analysis too complicated. However, at low C_t, i.e., when we can expect the importance of double layers interaction, the estimates suggest the weak logarithmic dependence of zeta potentials on $\tanh h/2\lambda$. Hence, we neglect this difference and assume that zeta potentials in the film do not change relative to those at large separation.

Now we can obtain the analog of the Bretherton equation (7) for electrokinetic flow. Integration of the velocity field in the flow rate balance (5) requires an integration in the local potential φ as seen in (2). With the small γ expansion in (23), this can now be done explicitly. With a nondimensionalization of all lengths on the capillary radius R and potentials on kT/e, this approximation to the flow rate balance (5) becomes

$$\frac{h^3}{6}[h_{xxx}+\text{Ca}_*\Phi_x\Phi_{xx}]-\text{Ca}\,h-\Delta\,\text{Ca}_*\Phi_x(h-2\lambda f)=\tfrac{1}{2}\text{Ca}_*\Phi_x^{\infty}(\Sigma-\Delta)-\text{Ca}, \tag{24}$$

where $f\approx\tanh(h/2\lambda)$ and we retain the same notation for nondimensional lengths and potentials. The bubble capillary number $\text{Ca}=\mu u_0/\sigma$ is based on the yet unknown bubble velocity u_0, the nondimensional bubble and capillary zeta potentials are represented through $\Sigma=\zeta_c-\zeta_b\equiv\zeta_c+|\zeta_b|$ and $\Delta=-\zeta_b-\zeta_c\equiv|\zeta_b|-\zeta_c$, and the electrokinetic capillary number Ca_* is introduced through the effective diffusion coefficient $D_*=(\epsilon\varepsilon_0/\mu)(kT/e)^2$ (about 0.48×10^{-5} cm^2/s for water at room temperature, such that $\text{Ca}_*=\mu D_*/\sigma R\approx0.6\times10^{-7}$ for our 0.5-mm-diam capillary). It should be noted that, with this initial nondimensionalization, the overall nondimensional voltage drop $V_0=eV/kT\gtrsim10^3$, such that capillary number for the film flow ($\sim\text{Ca}_*V_0$) is much larger than the extremely low electrokinetic capillary number Ca_*.

If the electric field strength Φ_x does not vary longitudinally in the flat portion of the film, Eq. (24) provides the bubble capillary number,

$$\text{Ca}=\frac{\text{Ca}_*}{2(1-h_0)}[\Phi_x^{\infty}(\Sigma-\Delta)+(\Phi_x)_0\Delta2(h_0-2\lambda f_0)], \tag{25}$$

where the subscript zero indicates the values taken in the flat film region. The first term in square brackets in (25) corresponds to the liquid flow in the capillary and is the same as (6) for the pressure-driven flow. The second term corresponds to the effect of the film flow and, depending on the sign of Δ, can reduce or enhance bubble speed. This term provides an order one correction to the bubble speed despite its higher order in h_0 because we expect an $O(1/h_0)$ field amplification in the film.

D. Current flux and longitudinal field

The relation between the electric field strengths Φ_x in the film and transition region, Φ_x^∞ in the capillary away from the bubble and the overall voltage drop can only be resolved with a current balance over the entire capillary. Since the current is the charge-weighted difference of mass fluxes of positive and negative ions, the bulk convection does not contribute to the current because of electroneutrality. Because we already neglect longitudinal variations in the bulk concentrations of ionic species, the main contribution to the total current will be due to the electromigrative fluxes. Since the mobility of each ion is proportional to the product of the molecular diffusivity and the ion charge, the proper effective diffusivities for the cations and anions of our model 1:1 electrolyte should be the (valency)^2 composition-weighted diffusivities of the true ions,

$$D_e^+ = \frac{1}{C_e}(C_0 D_{K^+} + 2C_a D_{H^+}),$$
$$D_e^- = \frac{1}{C_e}(C_0 D_{Cl^-} + 4C_a D_{SO_4^{2-}}). \tag{26}$$

In the film and transition regions, the potential Φ depends only on x due to the scales separation. This simplification allows a straightforward current balance for the model electrolyte. Invoking Bikerman's expression for double layer conductivity (which assumes non-interacting double layers),[12] we obtain

$$\frac{I}{2\pi\, Re[D^+ + D^-]C_t} = \Phi_x^\infty = 2\Phi_x[h + 2\lambda\beta], \tag{27}$$

where

$$\beta = \beta(C_e, C_s)$$
$$= \cosh\,\varphi_b^s/2 + \cosh\,\varphi_c^s/2 - 2$$
$$+ \frac{D^+ - D^-}{D^+ + D^-}(\sinh\,\varphi_b^s/2 + \sinh\,\varphi_c^s/2)$$
$$+ \frac{4D_*}{D^+ + D^-}(\cosh\,\zeta_b/2 + \cosh\,\zeta_c/2 - 2), \tag{28}$$

the effective diffusion coefficients of positive and negative ions

$$D^\pm = \frac{1}{C_t}(D_e^\pm C_e + D_s^\pm C_s)$$

are introduced only to simplify the notation. The difference in ionic mobility in the mobile and dense pats of the double layers is neglected. The last term in β corresponds to the current caused by the electrokinetic flow within the double layers and all other terms represent the contribution of electromigration. It is evident that β is large even at moderate values of interfacial potentials φ^s due to the Boltzmann distribution of concentrated ions in the double layers. The dimensionless double layer conductivity $2\lambda\beta$ hence will produce significantly lower potential gradient in the film and the transition region relative to the capillary,

$$\Phi_x = \frac{\Phi_x^\infty}{2[h + 2\lambda\beta]}, \tag{29}$$

even if the film thickness is of the order of 10–20 λ.

The complicated interdependence between interfacial surfactant concentration Γ and surface potential, which reduces to the simple relations (17) only at equilibrium and in the limit of $|\varphi_b^s| > 4$,[6] does not allow us to obtain a good approximation for the double layer conductivity β for interacting double layers. However, rough estimations suggest that it is proportional to $\tanh h/2\lambda$.

Under and near the bubble caps, the potential of the electroneutral solution $\Phi = \Phi(x,y)$ is governed by the Laplace equation $\nabla^2\Phi = 0$ with appropriate boundary conditions on the bubble interface and matching requirements in the film and at infinity. However, with our assumptions of constant bulk concentrations and immobile bubble interface, Eq. (29) can also be used as a rough approximation for the average field strength,

$$\Phi_x^{\text{caps}} = \frac{\int_0^h \Phi_x(x,y)(1-y)dy}{h(1-h/2)},$$

near the bubble caps if we replace h by $h(1-h/2)$ in the denominator of (29). Hence, approximating the bubble caps by hemispheres, we can integrate (29) along the entire capillary (omitting $2\lambda\beta$ outside the bubble and on the upper limit of integration) to relate the field strength in the capillary Φ_x^∞ with the overall dimensionless potential drop V_0:

$$V_0 \approx \Phi_x^\infty \left\{ \underbrace{L - l}_{\text{capillary}} + \underbrace{\frac{l-2}{2[h_0 + 2\lambda\beta]}}_{\text{flat film}} + \underbrace{\frac{\pi}{2\sqrt{2(h_0 + 2\lambda\beta)}}}_{\text{caps}} \right\}. \tag{30}$$

In Eq. (30), L and l are the nondimensional lengths of capillary and bubble, respectively, $h_0 \ll 1$ is the nondimensional thickness of the flat film under the bubble and only the lowest order in h_0 terms are kept.

For the same voltage drop, the ratio of resistances for the capillary with bubble (R_b) to that without one (R_0) is equal to the inverse ratio of the corresponding field strengths Φ_x^∞, and from (30) one obtains

$$\frac{R_b}{R_0} = 1 - \frac{l}{L} + \frac{l-2}{2L[h_0 + 2\lambda\beta]} + \frac{\pi}{2L\sqrt{2(h_0 + 2\lambda\beta)}}. \tag{31}$$

To test the model, we use Chen's measured value of $h_0 \approx 0.7\mu$m under the stationary bubble to fit our resistance data by (31) and (28) (with omitted D_* term) in Fig. 4. The

agreement is satisfactory for almost the entire experimental range of l for moving bubbles ($1.5 \lesssim l \lesssim 20$) even if caps resistance is neglected. In contrast, neglecting double layer conductivity results in about 30%–50% error in relative resistance. This verifies the applicability of the model 1:1 electrolyte to our system and allows us to extend (30) to a bubble in motion.

E. Modified Bretherton theory and comparison to experiment

Inserting (29) into Eq. (25) for the bubble speed and setting $f_0 \approx 1$, we obtain the bubble capillary number Ca in terms of the uniform film thickness under the bubble h_0:

$$\mathrm{Ca} = \frac{1}{2}\frac{\mathrm{Ca}_* \Phi_x^\infty [\Sigma(h_0 + 2\lambda\beta) - \Delta 2\lambda(1+\beta)]}{h_0 + 2\lambda\beta}, \tag{32}$$

where the factor $1 - h_0$ in the denominator of (25) has been approximated to 1. Equation (30) allows us to relate Ca with the overall potential drop V_0 and bubble length l,

$$\begin{aligned}\mathrm{Ca} &= \frac{\mathrm{Ca}_* V_0 [\Sigma(h_0 + 2\lambda\beta) - \Delta 2\lambda(1+\beta)]}{l - 2 + \pi(h_0 + 2\lambda\beta)^{1/2} + 2(L - l - 2)(h_0 + 2\lambda\beta)} \\ &\approx \frac{\mathrm{Ca}_* V_0 [\Sigma(h_0 + 2\lambda\beta) - \Delta 2\lambda(1+\beta)]}{l - 2 + 2L(h_0 + 2\lambda\beta)},\end{aligned} \tag{33}$$

or, in terms of ζ_c and $\zeta_c - \zeta_b$,

$$\mathrm{Ca} \approx \frac{\mathrm{Ca}_* V_0 [(\zeta_c - \zeta_b)(h_0 - 2\lambda) + 4\zeta_c \lambda(1+\beta)]}{l - 2 + 2L(h_0 + 2\lambda\beta)}. \tag{34}$$

It is evident that if the film is sufficiently thick ($h_0 \gg 2\lambda$) and the conductivity in the two double layers is negligible ($h_0 \gg 2\lambda\beta$), the bubble does not move ($\mathrm{Ca} \approx 0$) at $\zeta_c \approx \zeta_b$, as has been suggested in Sec. I for such simplest case. Accounting for conductivity in the double layers modifies this criterion, while Eq. (34) indicates that the highest bubble speed occurs for ζ_c and ζ_b of opposite signs at otherwise identical conditions.

With our scaling of all lengths with respect to the capillary radius, the nondimensional capillary length $L = 120$ (for our 3 cm length capillary) and $h_0 \sim 2\lambda\beta \sim 10^{-3}$, such that the cap resistance is negligible for relatively long bubbles. Capillary resistance, in general, should be kept despite its higher order in h_0. It also should be noted that (32) and (34) are valid with the restriction $h_0 > 4\lambda$. In the opposite case, all terms proportional to λ should be multiplied by the factor $\tanh(h_0/2\lambda)$.

By substituting (29) and (33) into the flow rate balance (24) and rescaling h on h_0 and x on $x_0 = h_0[6\,\mathrm{Ca}_* E(\delta + \Delta')]^{-1/3}$, one obtains the modified Bretherton equation,

$$\left[h_{xx} + a\left(\frac{k+1}{kh+1}\right)^2\right]_x = \frac{h-1}{h^3}\left[b + \frac{1-b}{kh+1}\right], \tag{35}$$

where

$$\begin{aligned} &k = \frac{h_0}{2\lambda\beta}, \quad a = \frac{\mathrm{Ca}_* E^2}{2}\frac{x_0^2}{h_0}, \quad b = \frac{\delta}{\delta + \Delta'}, \\ &E = \frac{V_0}{l - 2 + 2L(h_0 + 2\lambda\beta)}, \\ &\delta = 2\lambda\beta[\Sigma(k+1) - \Delta'], \quad \Delta' = \Delta\left(1 + \frac{1}{\beta}\right). \end{aligned} \tag{36}$$

In this notation, the bubble capillary number (34) becomes

$$\mathrm{Ca} = \mathrm{Ca}_* E \delta. \tag{37}$$

The second term on the left-hand side of (35) is important only for high field strength $E \gtrsim O(10^3)$. This corresponds to moderate bubble lengths ($l \lesssim 4-5$) for our range of applied voltages because $\mathrm{Ca}_* \sim O(10^{-7})$ and $x_0^2/h_0 \sim O(1)$ due to the required curvature matching with outer static cap solution. It is also evident that $\Delta' \gg \delta$ [and, consequently, the first term in the right-hand side of (35) is negligible] except when $\Delta \to 0$ and/or $k \to \infty$, or, in terms of h_0 and λ,

$$2\lambda\beta\Delta \ll h_0^2 \Sigma. \tag{38}$$

For our experimental conditions, this corresponds to $\Delta/k^2 \sim 10^{-4}-10^{-3}$, which means either extremely close ζ_c and $|\zeta_b|$ or total electrolyte concentration in excess of 10^{-2}.

Before solving (35), we examine several instructive but inaccurate limiting solutions. Let us consider first the extreme limit (38) for long bubbles. This implies, that we should omit $\sim a$ and $\sim 1 - b$ terms in (35), $\sim L$ term in the denominator of E, and $\sim \Delta$ term in (32). Equation (35) then becomes exactly Bretherton's problem (7). Using Bretherton's result (9) and invoking (36) and (37) results in a cubic equation which determines $(\mathrm{Ca})^{1/3}$:

$$\mathrm{Ca} = \frac{V_0}{l-2}\mathrm{Ca}_* \Sigma[0.64(6\,\mathrm{Ca})^{2/3} + 2\lambda\beta]. \tag{39}$$

In the limit of high concentrations, one should neglect $2\lambda\beta$ in (39) according to (38). This results in a cubic dependence of the bubble speed on the normalized field strength,

$$\mathrm{Ca}_{C_t \to \infty} = 36\left[0.64\,\mathrm{Ca}_* \frac{V_0}{l-2}(\zeta_c - \zeta_b)\right]^3. \tag{40}$$

However, because of low values of both zeta potentials in this limit and the extremely small Ca_*, (40) gives the bubble speed about 3–4 orders of magnitude lower than that detected in our experiments. The film thickness (9) in that limit remains larger than 4λ, such that underlying assumptions of Eqs. (32)–(35) hold.

In the opposite limit of low concentrations when $\Delta \to 0$, $\Sigma \approx 2\zeta_c$, and, for our range of applied voltages and bubble lengths, the exact solution of (39) indicates the dominance of the $2\lambda\beta$ term. However, it is impossible to satisfy the limiting condition (38) in such a case unless $\Delta \sim O(\lambda^2) \sim O(10^{-8})$ or if we do not take into account omitted $\tanh(h/2\lambda)$ factors in (32)–(35)—if we do not allow the film thickness to be smaller than 4 D lengths. If we relax the latter assumption, we obtain a similar upper estimate for the bubble speed

$$\mathrm{Ca}_{\Delta\to 0}\lesssim 36\left[0.64\ \mathrm{Ca}_*\frac{V_0}{l-2}2\zeta_c(1+\beta)\right]^3. \tag{41}$$

The lower bound for $\mathrm{Ca}_{\Delta\to 0}$ corresponds to $\beta=0$ in (41). Similar to (40) this estimate gives two orders of magnitude lower bubble speeds. At $C_t\approx 7.5\times 10^{-5}$ mol/l, which corresponds to $\zeta_c=|\zeta_b|$ in Fig. 2, the upper estimate (41) gives a speed even higher than the measured value at $C_0=10^{-5}$ mol/l (the corresponding $C_t=9.48\times 10^{-5}$ and at $C_0/C_t=10^{-6}/8.58\times 10^{-5}$ mol/l no bubble motion is detected), but, in contrast to the high concentration limit, calculated h_0 becomes smaller than 2λ for typical values of electric field strength for long bubbles. This implies that the omitted attractive double layers and repulsive van der Waals disjoining pressure should be appreciable in this limit.

Using the literature value[11] for the Hamaker constant $A=-10^{-20}$ J and h_0 calculated from (41), we estimate the van der Waals repulsive pressure $\Pi_{\mathrm{vdW}}=-A/6\pi h_0^3$ and the double layers attraction given by[11,3]

$$\Pi_{\mathrm{dl}}=16C_tkT\left\{\frac{2\gamma_c\gamma_b\cosh\ h_0/\lambda-\gamma_b^2-\gamma_c^2}{\sinh^2\ h_0/\lambda}\right\}, \tag{42}$$

where $\gamma_{b,c}=\tanh\varphi^s_{b,c}/4$. We found that, for such h_0 and C_t, $|\Pi_{\mathrm{dl}}|$ exceeds Π_{vdW} by several orders of magnitude and is comparable with capillary pressure σ/R. This means that such film under the bubble is extremely unstable and should collapse under the Coulombic attraction between oppositely charged capillary wall and bubble interface.

For shorter bubbles, the numerical solution of Eq. (35) (without $\sim 1-b$ terms but with full expression for E) confirms the validity of limits (40) and (41), only with $l-2$ in the denominator replaced by $\approx(l-1.52)$ for $l<4$, because the effects of quadratic in the V_0 term in (35) and that of h_0 in the denominator of E nearly cancel each other in our range of V_0 and l.

Since the low concentration limit is in play only at very small Δ and the limiting speed at high concentrations is found vanishingly small, we solve the modified Bretherton equation (35) with $b=0$ numerically for a range of a and k to find the dependence of bubble speed on V_0, l, and C_0 in our working range of concentrations. We integrate (35) in the positive x direction such that h blows up monotonically. As h increases, the effect of $\sim a$ term vanishes in (35). This indicates that the Maxwell stress becomes negligible in the cap region where the capillary forces dictate a constant curvature cap. Similar to the classical Bretherton problem, the solution blows up quadratically as $x\to\infty$ but the asymptotic curvature κ_∞ depends on a and k. In dimensional form, this curvature must be equal to the inverse capillary radius, which is the basis of our matched asymptotic analysis. By fitting the obtained data on κ_∞ and invoking the indicated curvature matching[2,4] [used to derive (9)], we deduce an approximate analytical expression for h_0. It only slightly deviates from the numerical result over all ranges of concentrations and field strengths:

$$\frac{h_0}{2\lambda\beta}=k_0(B)=\left[\frac{B}{c+B^{2/5}}\right]^{2/3}. \tag{43}$$

In (43), $c=(0.407/0.643\,42)^{3/2}\approx 0.503$ is a numerical constant obtained from the curvature matching, and B is the concentration-normalized field strength:

$$B=B_EB_C,\quad B_E=\frac{2\ \mathrm{Ca}_*E_*}{2-\mathrm{Ca}_*E_*^2},\quad B_C=6\Delta'\left[\frac{0.407}{2\lambda\beta}\right]^{3/2}, \tag{44}$$

where $E_*=V_0/(l-2+8L\lambda\beta)$ and $\Delta'=\Delta(1+1/\beta)$. The subscripts C and E indicate the dominant dependencies. B_C depends only on concentrations of ionic species and B_E on the average field strength in the film E_* (which, for the longest bubbles, only weakly depends on C_t and C_s). For our range of bubble lengths and field strengths, $\mathrm{Ca}_*E_*^2$ reaches 2 only for the shortest bubbles with $l<2$, where our long bubble model obviously cannot be applied. The film thickness $h_0\sim(\Delta E_*)^{(2/3)}$ at low electrolyte concentrations and $h_0\sim(\Delta E_*)^{(2/5)}(2\lambda\beta)^{(3/5)}$ in the opposite limit. For our experimental conditions, typical values of B for moving bubbles with $l>2$ belong to the range $O(10^{-2})$ to $O(10)$. It is evident from (43) and (44) that in this range none of the above limits is reached because $B^{2/5}$ is about the same order as c.

Equation (33), with h_0 defined by (43) and (44), then provides the bubble capillary number:

$$\mathrm{Ca}=\frac{\mathrm{Ca}_*V_0[\Sigma(h_0+2f_0\lambda\beta)-\Delta 2f_0\lambda(1+\beta)]}{l-2+2L(h_0+2f_0\lambda\beta)}, \tag{45}$$

where $f_0=\tanh(h_0/2\lambda)$ factors have been included to capture the proper decay of speed at low concentrations. In general, (45) does not admit simple scalings with respect to experimental parameters. However, it is possible to partially separate effects of concentrations and concentration-normalized field strength B by rewriting (45) as

$$\mathrm{Ca}\times F_C=\frac{B[k_0(B)+F_1]}{(1+F_2)(1+F_E)}, \tag{46}$$

where

$$F_C=\frac{B_C}{2\lambda\beta\Sigma}=1.558(2\lambda\beta)^{-5/2}\frac{\Delta'}{\Sigma},$$

$$F_1=\tanh(\beta k_0)\left[1-\frac{\Delta'}{\Sigma}\right],$$

$$F_2=\frac{4L\lambda\beta(k_0-1)}{l-2+8L\lambda\beta},$$

$$F_E=\left(\frac{1}{4}+\frac{2B^2}{B_C^2\mathrm{Ca}_*}\right)^{1/2}-\frac{1}{2}=\frac{\mathrm{Ca}_*E_*^2}{2-\mathrm{Ca}_*E_*^2}.$$

It is evident from (46) that F_C is a strong function of C_t. Parameters F_2 and F_E are of the order of $O(10^{-2})$ for the long bubbles (with $l\gtrsim 10$ for moderate voltages within bubble motion window) and begin to differ appreciably from zero at intermediate bubble lengths ($l\lesssim 4$ for the typical experimental conditions). For the same conditions, F_1 ranges from about 0.5 to 0.95 [that is of the same order as $k_0(B)$ for

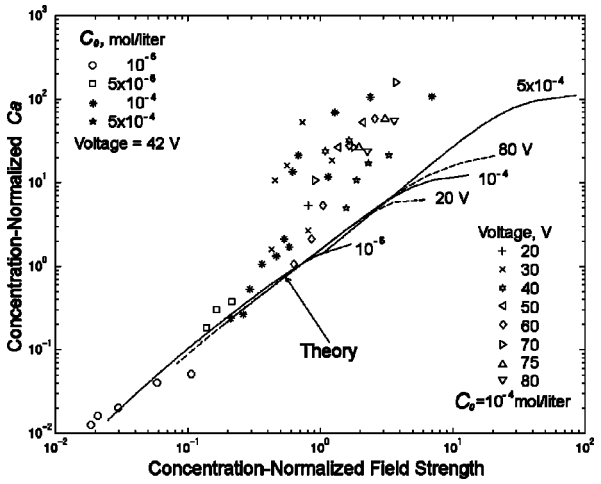

FIG. 10. Collapse of the measured bubble speed by the correlations of our theory with normalized field strength B. The low-field data typically correspond to long bubbles where the theory is more valid. The lines correspond to the predictions of Eq. (47): (—) $V=42$ V and indicated values of C_0; (---) $C_0=10^{-4}$ mol/l and indicated applied voltage.

average and long bubbles]. In such case, it depends weakly on both B and C_t, while trends to zero at both low and high concentration limits.

In Fig. 10, we present the approximate normalization of bubble speed by (46). All our data on bubble speed are plotted in the coordinates $\mathrm{Ca}\times F_C$ versus the normalized field strength B. The proposed dependence successfully collapses our data for various C_0 and V for long bubbles. Even for shorter bubbles, the data scattering does not exceed 20%, except several data points from the 42 and 30 V runs at $C_0=10^{-4}$ mol/l.

The theoretical curves, also plotted in Fig. 10, represent the range of experimental conditions studied. It is evident that within the experimental window for bubble motion, all curves, except their flat portions, are very close to each other. The flat parts approach the limiting bubble speed [the limit $h_0\to\infty$ of Eq. (45)]. They are significant only for short bubbles ($l\lesssim 3$) even at the highest V and C_0 of our experiments, where the long-bubble model cannot be applied. Hence, the right-hand side of (46) depends mostly on B for average and long bubbles and, within the working range of V and C_0, it can be approximated by a power law, such that bubble speed becomes

$$\mathrm{Ca}\approx 1.32B^{1.24}F_C^{-1}=8.37B_E^{1.24}(2\lambda\beta)^{0.76}\Sigma\left[\Delta\left(1+\frac{1}{\beta}\right)\right]^{0.24}, \tag{47}$$

where $B_E\approx \mathrm{Ca}_* E_*$ is defined by (44). It should be noted that the sequence of limits $B^{2/5}\ll c$ and $\beta k_0\ll 1$, $B^{2/5}\ll c$ and $k_0\ll F_1$, and $B^{2/5}\gg c$ and $k_0\gg F_1$ corresponds to increase in B and C_t from zero and C_t^c, low B and C_t values, and large B and C_t values. This sequence yields the powers 5/3, 1, and 1.4 sequence for the exponent of B in (47). While none of the limits is strictly applicable within the experimental range, it seems that terms of the same order in (44) and (46) conspire to produce some ''average'' power in (47).

As seen in Fig. 10, Eq. (46) or (47) satisfactory represents the normalized bubble speed at low $C_0=10^{-5}$ and 5×10^{5}. For $C_0=10^{-4}$, only the speed of the longest bubbles is captured (low $B\lesssim 0.5$), while at higher $B\gtrsim 1$ and $C_0=5\times10^{-4}$, even for long bubbles, the normalized bubble speed $\mathrm{Ca}\times F_C$ is underestimated. Of course, (46) cannot be applied for short bubbles with $l<2$, but strong deviations already begin at moderate field strengths (for the 42 V and 10^{-4} mol/l run, it corresponds to $l\sim 8$). At the same time, the increase in data scattering indicates that our model may not provide the proper scaling with respect to field strength or C_t.

Simplified Eq. (47) and the dependencies of β, λ, and zeta potentials on C_t suggest that $\mathrm{Ca}\sim(C_t-C_t^c)^{0.24}$ near the lower bound of the bubble motion window (which is defined by the condition $\Delta=0$) and $\mathrm{Ca}\sim C_t^{-1.38}$ in the high-concentrations limit. However, the average power law (47) does not necessary hold in these limits, and we use the full expression (46) to explore the ability of our model to predict the dependence of bubble speed on the electrolyte concentration alone. Since all our data for varying C_0 corresponds to the 42 V applied, we select the speed data for long bubbles of identical or very close lengths for comparison. Because of the small number of such data points, data corresponding to nearly identical V/l and different C_0 ($V/l\approx E_*$ for long bubbles) are also plotted in Fig. 6 along with the theoretical predictions. As seen in Fig. 6, for long bubbles with low electric field, (46) satisfactorily captures the dependence of bubble speed on electrolyte concentration, as well as the window for bubble motion.

The speed saturation at high voltages is not captured: Eq. (45) gives a limiting linear dependence of Ca on V_0. Since our voltage-velocity data of Fig. 5 correspond to intermediate bubble lengths ($l=4$ and $l=5.2$), where the proposed theory strongly underestimates the bubble speed, we cannot even say whether the voltage-velocity scaling is captured.

The discrepancies at moderate and high field strengths can arise for several reasons. The main one seems to be the violation of the long-bubble assumption—at those lengths, the front and back caps begin to feel each other, and concentrations and electric field gradients do not vanish within the flat portion of the film. Depending on the relative mobility of positive and negative ions and the intensity of convection in the film, the longitudinal gradients of electrolyte and surfactant concentrations can oppose or assist bubble motion. A complete analysis including longitudinal gradients is too complicated for our multicomponent system and cannot be done within the long-bubble approximation. Our estimates, however, suggest that the effect is opposite for short and long bubbles. For short bubbles, the preferable convection of anionic surfactant within the wall double layer and electromigration of absorbed surfactant molecules along the interface result in additional enhancement of interfacial surfactant concentration at the front cap. In contrast with the usual Marangoni effect, which can only make the interface immobile, the addition of electromigrative surfactant fluxes can result in negative interfacial velocity (roughly proportional to $-\mathrm{Ca}_* E^2 h/l$), assisting in bubble motion and preventing creation of charge separation along the bubble.

For long bubbles, this effect diminishes and even immobilization of interface may not be reached. Hence, in time, positive ions accumulate near the back cap and negative ones at the front, creating an opposing potential gradient. Since axial diffusion for long bubbles is incapable of countering this effect, long bubbles can decelerate. Any stoppage in the applied voltage allows axial diffusion to remove this charge separation. The ratio of the measured bubble velocity after voltage is reapplied to that before deceleration, as shown in Fig. 9, scales linearly with respect to $\tau^{1/2}/l_b$, where τ is the time delay before the voltage is reapplied. To render $\tau^{1/2}/l_b$ nondimensional, we use $D=10^{-5}$ cm^2/s, which gives the correct order of magnitude for diffusivity of all ions except H^+ in our working solution. The exact value of D is not important for our scaling purposes. This linear scaling is consistent with the diffusion smoothing of the concentration gradients in the film.

V. CONCLUSIONS

While we have mapped out the windows within which electrokinetic displacement of bubbles is possible and observe very high bubble speeds when film flow is stopped by the growing double layers, our results are only applicable for cylindrical capillaries and not for the noncircular cross sections more common in microlaboratory and microreactor applications. As shown in our study of square capillaries,[5] there are corner regions where thick films exist. In electrokinetic flow, much of the current and electrokinetic flow would then go through the corner region and the thin film regions away from corner which are essentially stagnant. This suggests the flow bypass through the corners will be equal to the flow behind the bubble and the bubble will remain stationary. This can be avoided if one can increase λ or decrease thickness in the corner region such that the twin double layers again overlap to reduce the flow. However, this requires an extremely low C_0 as the film thickness in the corner region is two or three orders of magnitude larger than the micron-level thickness in a cylindrical capillary. This implies that a very high, perhaps impractical, voltage is required to drive the liquid away from the bubble. A more attractive solution may be to externally introduce a normal field to enlarge the double layer thickness at the corners.

ACKNOWLEDGMENTS

This work is supported by NSF grant on ''XYZ on a Chip.'' Eric Sherer, an undergraduate from Caltech, carried out some of the experiments.

[1] R. F. Probstein, *Physicochemical Hydrodynamics—An Introduction* (Butterworths, Boston, MA, 1989).
[2] J. Ratulowski and H.-C. Chang, ''Marangoni effects at trace impurities on the motion of long gas bubbles in capillaries,'' J. Fluid Mech. **210**, 303 (1990).
[3] H. J. Schultz, *Physico-chemical Elementary Processes in Flotation* (Elsevier, New York, 1984).
[4] F. P. Bretherton, ''The motion of long gas bubbles in tubes,'' J. Fluid Mech. **10**, 166 (1961).
[5] J. Ratulowski and H. C. Chang, ''Transport of air bubbles in capillaries,'' Phys. Fluids A **1**, 1642 (1989).
[6] J. T. Davies and E. K. Rideal, *Interfacial Phenomena* (Academic, London, 1961).
[7] K. P. Tikhomolova, *Electro-osmosis* (Horwood, NJ, 1993).
[8] J. D. Chen, ''Measuring the film thickness surrounding a bubble inside a capillary,'' J. Colloid Interface Sci. **109**, 341 (1986).
[9] V. G. Levich, *Physicochemical Hydrodynamics* (Prentice–Hall, Englewood Cliffs, NJ, 1962).
[10] D. V. Sivukhin, *Elektrichestvo* (Nauka, Moscow, 1979).
[11] J. N. Israelachvili, *Intermolecular and Surface Forces* (Academic, London, 1991).
[12] S. S. Dukhin, *Elektroprovodnost' i Elektrokineticheskie Svojstva Dispersnyh System* (Naukova Dumka, Kiev, 1975).